May 17th, 9:20 AM

A 3D Study of an Intake Air-Core Vortex Structure Using PIV & Flow Visualization

V. Naderi
vadoud.naderi@mail.mcgill.ca

Susan Gaskin
McGill University, susan.gaskin@mcgill.ca

Recommended Citation

Naderi, V. (2018). A 3D Study of an Intake Air-Core Vortex Structure Using PIV & Flow Visualization. Daniel Bung, Blake Tullis, 7th IAHR International Symposium on Hydraulic Structures, Aachen, Germany, 15-18 May. doi: 10.15142/T3K93V (978-0-692-13277-7).

7th International Symposium on Hydraulic Structures Aachen, Germany, 15-18 May 2018
ISBN: 978-0-692-13277-7 DOI: 10.15142/T3K93V

A 3D Study of An Intake Air-Core Vortex Structure Using PIV & Flow Visualization

V. Naderi[1], S. Gaskin[2]
[1] *University of Tabriz, Department of Water Science and Engineering (PhD) and McGill University (GRT)*
[2]*McGill University, Department of Civil Engineering and Applied Mechanics, Montreal, Canada*
E-mail: vadoud.naderi@mail.mcgill.ca

Abstract: *A free surface vortex is a mass of water rotating around an axis which at a low intensity of rotation results in a dimple at the water surface and at a high intensity of rotation can result in an air-core at its center. Air-core vortices can occur at intakes withdrawing water from reservoirs. Existing vortex models provide general information about the symmetric vortex structure. The aim of the present study was to examine the vortex structure at the critical submergence condition occurring in an approach flow which results in a non-symmetric velocity distribution and structure of the vortex throughout the flow depth. A steady strong air-core vortex over a bottom intake was created in a recirculating flume in which the water depth, mean velocity of the approach flow, and intake discharge could be adjusted. A combination of flow visualization and detailed PIV data allowed the asymmetric structure of the strong air-core vortex in an approach flow to be studied. Flow visualization was used to observe the formation and evolution of the three-dimensional structure of the air-core. Planar particle image velocimetry (PIV) was used in a series of horizontal and vertical planes to reconstruct the three-dimensional structure of the (strong air-core) vortex. Analysis of this data revealed an asymmetric vortex structure in the horizontal plane throughout the flow depth due to the approach flow creating a mixing zone upstream of the vortex.*

Keywords: *Vortex structure, asymmetric vortex, velocity distribution, bottom intake, PIV, flow visualization.*

1. Introduction

Free surface vortices occurring at the intakes of hydraulic systems such as hydropower stations and pump intakes can cause serious technical problems in the hydraulic systems such as air entrainment, vibration and the deterioration of pump or turbine performance. Most investigations of free surface vortices have focused on the risk of air entrainment at given flow parameters. The surface disturbance caused by a vortex increases from small coherent surface swirling motions to fully developed air-core vortices as the vortex strength increases. Denny (1956) named and characterized different stages in development of air entraining vortex. Figure 1 shows the classification of different vortex types by Hecker (1987). As the distance between the top of the intake and the free surface reduces, the strength of the vortex increases. A critical submergence is defined as the depth just greater than that at which air entrainment occurs.

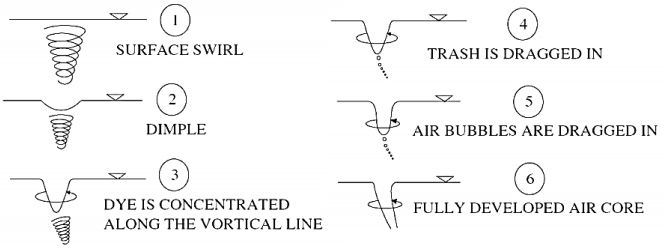

Figure 1. Vortex type classification (Hecker 1987).

Previous studies predicting critical submergence have investigated the effect of anti-vortex devices on the characteristics of the vortices and on the critical submergence under different conditions. Conditions investigated include a change in the angle of the approaching-flow to the direction of the main flow, use of different shapes of the intake mouth for different flow conditions, adoption of different intake cross sections and displacement of the intakes vertically or horizontally. The majority of these studies have been experimental or analytical, e.g., Anwar (1968), Gulliver and Rindels (1987), Hite and Mih (1994), Jain et al. (1978), Borgei and Kabiri-Samani (2010), Naderi et al. (2013, 2014) and Shemshi and Kabiri-Samani (2017). In addition to the studies on critical submergence, theoretical and experimental investigations have been conducted on the hydraulic characteristics of vortices. The classic Rankine (1858) vortex model describes a free surface vortex with a tangential velocity of:

$$V_\theta = \begin{cases} \frac{\Gamma r}{2\pi {r_m}^2} & , r \le r_m \\ \frac{\Gamma}{2\pi r} & , r > r_m \end{cases} \quad (1)$$

Where V_θ is the tangential velocity, r_{m} is the radius at the maximum tangential velocity and Γ is the maximum circulation of the vortex. Odgard (1986) used Burgers (1948) Model of stable vortex, obtained by balancing axial stretching with viscous diffusion, assuming a linear profile of axial velocity from the bed to the free surface. Using the Navier-Stokes equations, the tangential velocity is predicted as:

$$V_\theta = \frac{\Gamma}{2\pi r}\left[1 - \exp(-1.25\ \left(\frac{r}{r_m}\right)^2)\right] \quad (2)$$

Mih (1990), using a large number of experimental data, modified the Rankine vortex model and proposed a formula for predicting tangential velocity as:

$$V_\theta = \frac{\Gamma}{2\pi r_m}\frac{2\left(\frac{r}{r_m}\right)}{1+2\left(\frac{r}{r_m}\right)^2} \quad (3)$$

Wang et al. (2011) further modified Eq. (3) to produce a better fit to the data and expressed it as:

$$V_\theta = \frac{\Gamma}{2\pi r_m}\frac{m_1\left(\frac{r}{r_m}\right)}{1+m_2\left(\frac{r}{r_m}\right)+\left(\frac{r}{r_m}\right)^2} \quad (4)$$

This equation is known as the modified Mih formula, where $m_1 = 0.928$ and $m_2 = -0.7$. Several experimental studies of the velocity distribution or vortex flow field have used Acoustic Doppler Velocimetry (ADV) or Laser Doppler Anemometry (LDA) (Hite and Mih 1994 and Sarkardeh et al. 2010). The main disadvantage of using such point measurement systems is the lack of spatial information. Particle Image Velocimetry (PIV) improve on this deficiency. An advantage of PIV in turbulent flow fields is that turbulence statistics, such Reynolds stresses, can be derived from the two-dimensional velocity fields (Wang et al. (2011)). Li et al. (2008) used PIV to get a laminar flow field of a free surface vortex. Rajendran and Patel (2000) and Okamura et al. (2007) studied time-averaged velocity fields of a spiral vortex at a pump-intake using PIV. Suerich-Gulick et al. (2014) have studied the vortex flow field using PIV to develop an analytical model. Moller et al. (2015) and Mulligan et al. (2016) have conducted experimental studies about air-entraining vortices and effect of the approach geometry on the vortices providing useful information about the vortex structure subsequently. However, the detailed flow structures of a strong air-core vortex under critical submergence have yet to be explored. A better understanding of this phenomenon is required both for basic research and for applied engineering systems.

In the present study, a stable air-core vortex under the critical submergence condition for a bottom vertical intake located in a wide flume was developed. PIV was used to obtain horizontal sections of the velocity vector fields at intervals over the depth in addition to two vertical sections upstream of the intake. This allowed for a detailed description of the three-dimensional structure of vortex and the approach flow. The observations were validated by using the tangential velocity in the horizontal plane.

2. Experimentation

2.1. Water Channel and Intake System

A glass-walled and Plexiglas-bottomed re-circulating water channel 4.95 m long and 1 m wide situated at the Laser Laboratory of Department of Civil Engineering, National Chung Hsing University, Taiwan was used for the experiments. Reservoirs at each end of the water channel, one for the inlet flow (1.55 m long, 1 m wide and 1.4 m deep) and the other for outlet flow (1.55 m long, 1 m wide and 1.4 m deep), were installed. In the lower region of the upstream reservoir, a multi-layered and perforated energy dissipating section ensured the inflow was uniform and free of circulation (energy dissipation system includes a large number of vertical pipes with 5mm diameter and 100 mm height). A digitally-controlled centrifugal pump circulated the flow from the upstream reservoir through the test section to downstream reservoir and around again. The test section dimensions were 2 m long, 1 m wide and 0.4 m high. To create a steady air-core vortex, a horizontal plate with a streamlined leading edge and dimensions of 2 m long, 1 m wide and 10 mm thick was placed parallel to the bottom glass of the water channel whose vertical position could be adjusted (in the range of 10 to 100 mm) to modify the submergence.

A vertical pipe having an inner diameter of 94 mm was installed on the midline flush with the top surface of the adjustable submergence plate and 1.25 m from its leading edge. It passed through the bottom Plexiglas of the water channel where a second digitally-controlled centrifugal pump controlled the flowrate, thus forming a bottom intake system. The water extracted through the bottom intake passed through an upside down U-shaped pipe and was expelled into the end of the downstream reservoir. To enhance the asymmetry of the approach flow and promote the formation of a strong air-core vortex, a vertical plate (1.75 m long, 0.5 cm high and 10 mm thick) was placed parallel to the downstream left wall at a distance of 208 mm. The intake was, therefore, 282 mm from the left plate and 500 mm from the right-side wall (see Figures 2 and 4). In the present study, the water depth of approach flow over the horizontal plate was set to 118 mm. The mean velocity of the approach flow was set to 66 mm/s and the bottom intake flow was set to be 665 mm/s. Under these conditions, a strong stable free-surface vortex with an air core is produced having a critical submergence of 118 mm.

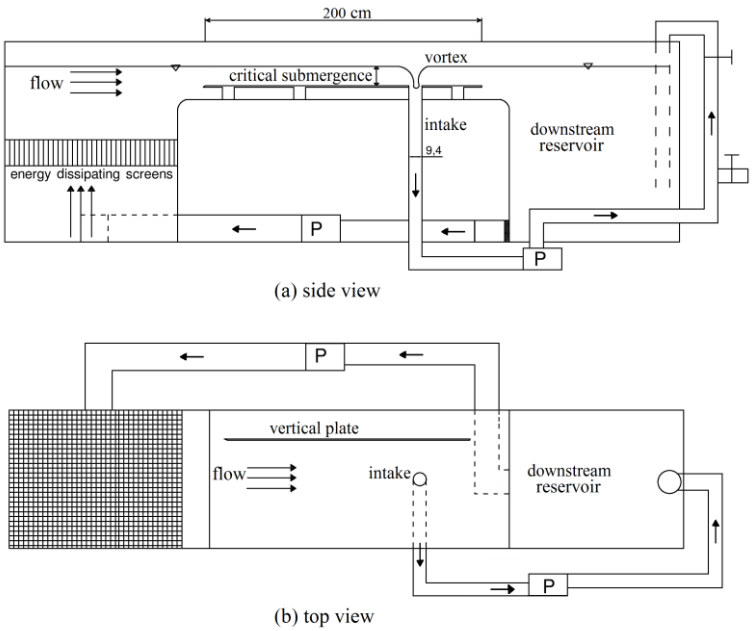

Figure 2. Schematic diagram of experimental setup: (a) side view and (b) top view.

2.2. PIV and Flow Visualization Setup

A continuous Innova 300C Argon laser was used for illuminating the fields of view by providing a 2-mm thick light sheet. Each horizontal view was produced from eight different fields of view (FOVs) (see Figure 3). The high-speed camera, a Phantom Miro eX4 with an 800×600 pixels resolution equipped with a Nikon 50mm camera lens, was oriented perpendicular to the laser sheet. The camera and laser pulses were synchronized at 100 fps with an exposure time of 10 ms. The total acquisition time for each test was 42 s corresponding to 4411 images. The camera was placed under the flume for horizontal laser sheet images and on the right side of the flume for the vertical images. Aluminum powder, having a purity and particle diameter of 99% and 1µm, respectively, was used as tracer particles. Horizontal PIV images were obtained at three elevations, 0.25h, 0.5h and 0.75h, where h is the water depth in the flume (fixed at 118 mm in all the experimental tests) (See Figure 4 (a)). The PIV measurements producing vertical sections parallel to the flume walls were obtained at two locations, Y=0 cm and Y=6.5 cm from the intake axis (See Figure 4 (b)).

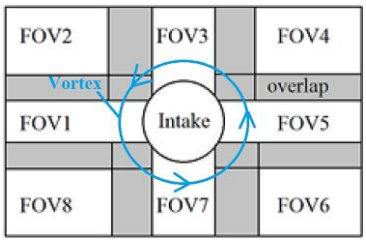

Figure 3. All the FOVs at each horizontal PIV elevation (plan view).

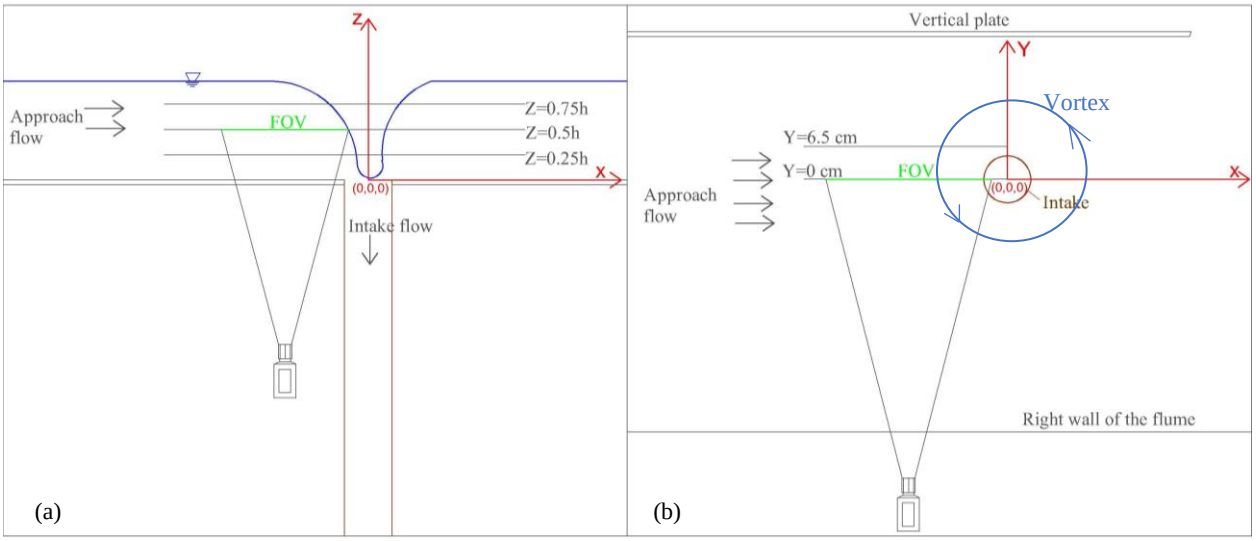

Figure 4. Schematic of PIV and flow visualization setup; (a): Horizontal PIV images (side view of the flume); (b) Vertical PIV images (plan view of the flume).

2.3. Coordinate System

The origin of the coordinate system is located at the origin of the vortex core. The horizontal axis, X, is in the stream-wise direction of the uniform flow of the channel and parallel to the horizontal plate, the transverse (or span-wise) axis, Y, is horizontal and normal to the X-axis (positive to the downstream left), and the vertical axis, Z, is oriented upwards. A cylindrical coordinate system is also used in which in the horizontal plane the radial velocity, V_r, is outwards and the tangential velocity, V_θ, is perpendicular to the radial velocity (anticlockwise) and tangent to the velocity of the rotating fluid.

3. Experimental Results and Discussion

3.1. Flow Visualization

This work focuses on the 3D structure of a vortex, a steady, incompressible and asymmetric rotational flow, under approach flow and critical submergence conditions. The focus of the present study is to elucidate the flow structure of an air-core vortex in an approach flow in general with a more comprehensive study of the flow field upstream of the vortex. A schematic view of the flow structure of the mixing zone due to the interaction of the vortex and approach flows is shown in Figure 5. The vortex flow particles move along helicoidal path-lines around the vortex core (with a small displacement towards the (+x, -y) direction) in which counterclockwise rotation of the vortex is in the –Y direction. Thus, on the right and left sides of the vortex core, all the vortex flow particles move in the positive and negative X-directions, respectively (see Figure 4). Furthermore, the horizontal velocity component of particles in the X-direction, U, on the right and left side of the vortex are positive (+U) and negative (-U) values, respectively. At the upstream face of the vortex, the approach flow moves in the positive X-direction, $+U_{app}$, and decelerates as it nears the vortex and meets the tangential vortex flow. This creates a turbulent mixing zone centered on the line where the approach flow velocity is reduced to zero, which occurs on the left side of flume where the approach flow and tangential velocity are in opposing directions. As shown in Figure 5, the steady air-core vortex flow obstructs the flow, in a manner similar to that of a pier in a river flow, causing a long curved horizontal horseshoe vortex in the mixing zone spanning half the flow width. In this mixing region, the horizontal vortex flow rotates about an axis in the diagonal plus X minus Y-direction. The mixing zone flow particles, therefore, move along a helicoidal path, starting from the left side of the flume upstream of the air-core vortex and spiraling in to join the air-core vortex in the middle of the flume where the vortex and the approach flow velocities are aligned. The approach flow particles flow above and below this horizontal vortex at relatively low and high speeds, respectively. The exact location of the horizontal mixing zone vortex varies over time. The flow visualization technique used in both horizontal and vertical planes revealed more information about the physics of the mixing zone and its effect on the main vortex structure.

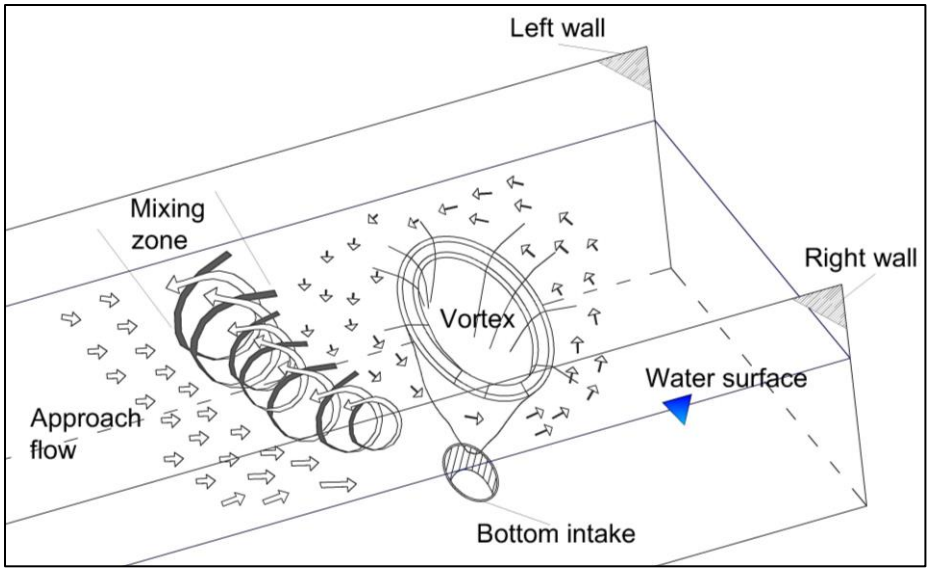

Figure 5. Schematic diagram of vortex, mixing zone and approach flow.

In previous studies on the vortex structure based on the Rankine Vortex Model, it is usually assumed that the fluid moves in a closed completely symmetric and circular path. However, the effect of the approach flow is to cause the flow's trajectory to be asymmetric. Figure 6 shows a series of fine resolution streak-line images captured using the flow visualization technique for all the FOVs of Figure 3 at a depth of $\frac{h}{z} = 0.75$. Note that all the adjacent field of views shown in Figure 6 have 30% overlap. Particle path-lines shown in Figure 6 illustrate the velocity of the fluid: the longer the path the higher the velocity. A detailed inspection of Figure 6 reveals that the path-lines in FOVs #2 and #1 are shorter than those of the other FOVs, thus have a lower velocity. In a plan view, it can be observed that as the approach flow and the tangential velocity of the air-core vortex approach each other in the mixing zone (FOVs #1 and 2), both velocities start to decrease and reach zero along the yellow line shown in Figure 6. Images using the flow visualization technique for vertical FOVs are shown in Figure 7. The evolution of the flow structure in the mixing zone is shown by the vertical sections at Y=0 cm and Y=6.5 cm in three images at four second time intervals. For the vertical FOV aligned with the intake, Y= 0 cm, a small horizontal eddy (-Y vorticity) was observed for t = 0 s in which the approach flow was dominant shown by the longer streak-lines (Figure 7(a)). In Figure 7(b) four seconds later, the initial structure breaks down into a vortex pair; two small horizontal vortices with opposite-signed vorticity form in which the approach flow divides flowing above and below the vortex pair. By t = 8 s, the vortex pairs are joined again into a small coherent eddy (-Y vorticity) on the upper side of the intake (Figure 7(c)). In summary, the vertical flow visualization images at Y=0 cm illustrates the high velocity of the flow below the horizontal mixing zone vortex. The vertical FOV at Y=6.5 cm shows the air-core vortex flow particles moving in the negative X-direction (Figure 7 (d, e & f)). In these images, the mixing zone rotating core can shift in the X-direction and is on average located further from the air-core vortex flow. These images show that the mixing zone vortex is unsteady and varies in strength and location. The instantaneous flow pattern captured in Figures 6 and 7 are further supported by the time averaged PIV measurements shown later in Figures 8 and 9.

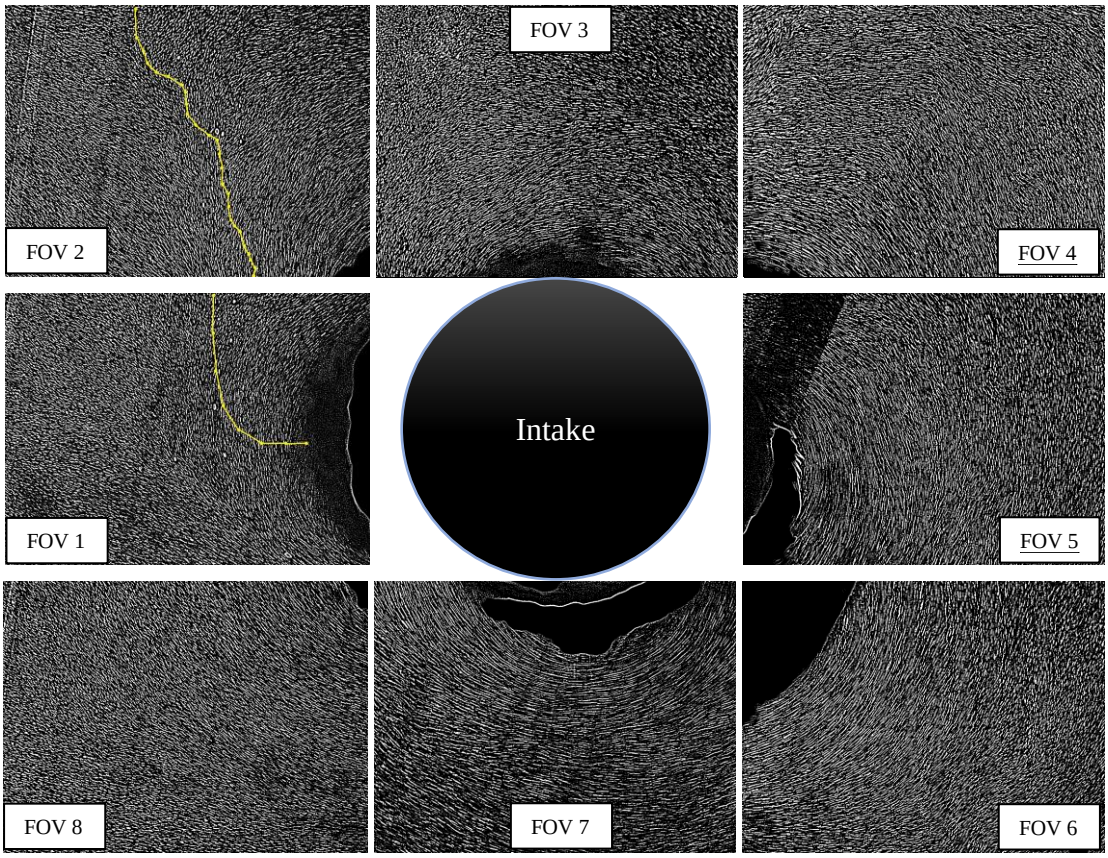

Figure 6. Instantaneous streak-line images for horizontal FOVs at Z=0.75h.

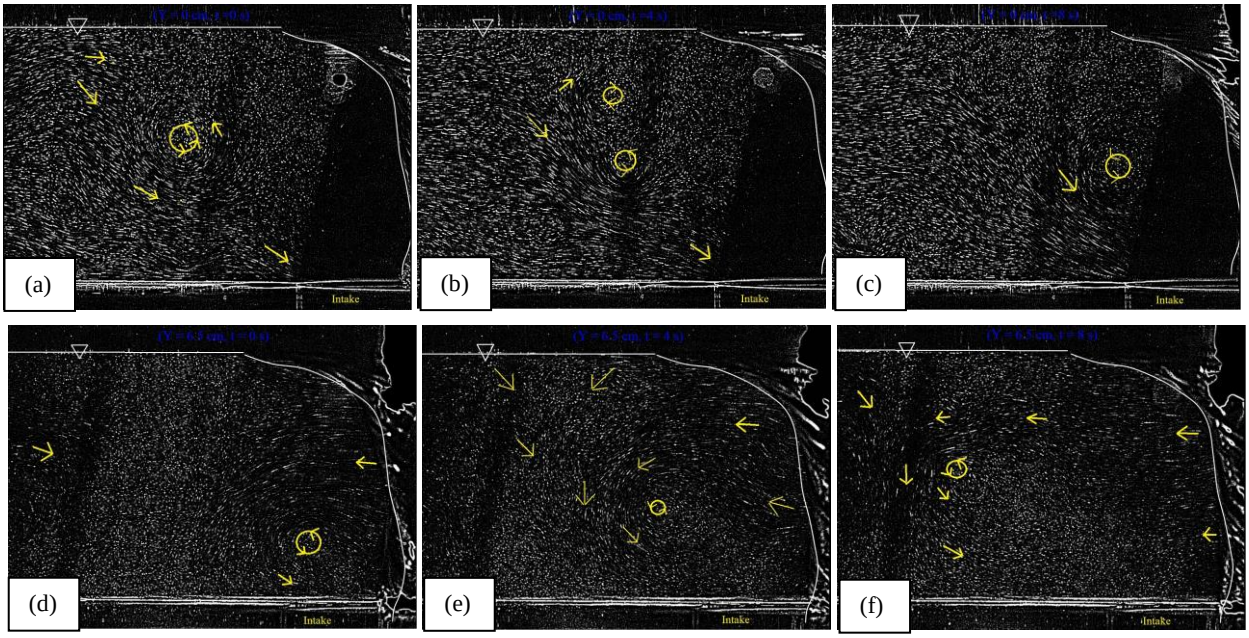

Figure 7. Instantaneous streak-line images for vertical FOVs at: (a) Y=0 cm at t= 0s; (b) Y=0 cm at t= 4s; (c) Y=0 cm at t= 8s; (d) Y=6.5 cm at t= 0s; (e) Y=6.5 cm at t= 4s; (f) Y=6.5 cm at t= 8s.

3.2. Velocity Fields by PIV

Time averaged velocity vector fields for each FOV of Figure 3 are obtained using the PIV technique. All eight FOVs are merged into one in Figure 8 to show the time averaged velocity vectors of the air-core vortex at Z = 0.75h. The flow pattern indicates the asymmetric structure of the air-core vortex due to the effect of the approach flow (with higher velocities downstream right). The mixing zone is recognized as the white diagonal region upstream of the vortex core in which the velocity in the downstream direction is zero. The time averaged vertical PIV velocity fields are shown in Figure 9 in which the interaction of the approach flow and the vortex flow is seen. The instantaneous streak-lines seen in the vertical section at y= 0 cm in Figure 7 illustrate a recirculation cell with -Y rotation about a span-wise axis located approximately at mid-depth. This results in a sweep of flow below the recirculating cell due to alignment of the velocities and a reduction in the flow velocities above the cell as the velocities are in opposing directions. In the time averaged PIV velocity vector field at Y=0 cm (Figure 9 (a)), a high velocity region is seen at lower depths and at higher elevations a stagnation region is seen upstream of the air-core vortex. In the time average PIV velocity vector field at Y=6.5 cm (Figure 7 (b)), a horizontal vortex is clearly seen upstream of the air-core vortex (X = -7.5 cm) and at 1/3 the depth (Z = 4 cm). Above this, high velocity vectors in the upstream direction are seen due to the rotation of the air-core vortex. The location of the mixing zone line, defined as the location of zero velocity in the X-direction (the velocity is vertically down), is located upstream of the air-core vortex at X = -15 cm. This can be compared to a location of X = -5 cm in the Y= 0 cm section.

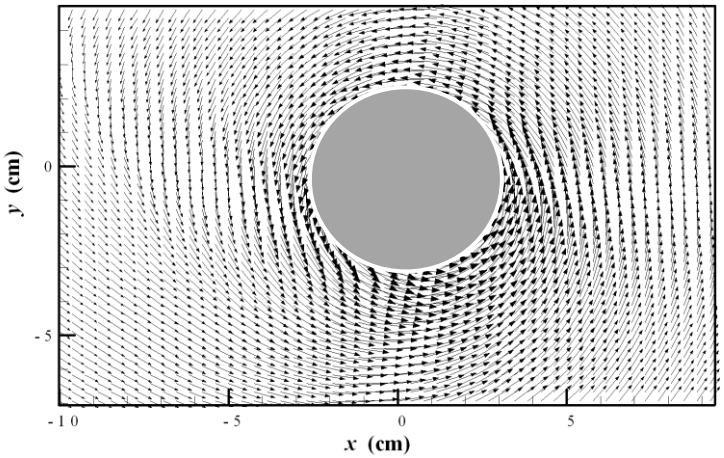

Figure 8. Velocity vector field of horizontal PIV at Z=0.75h.

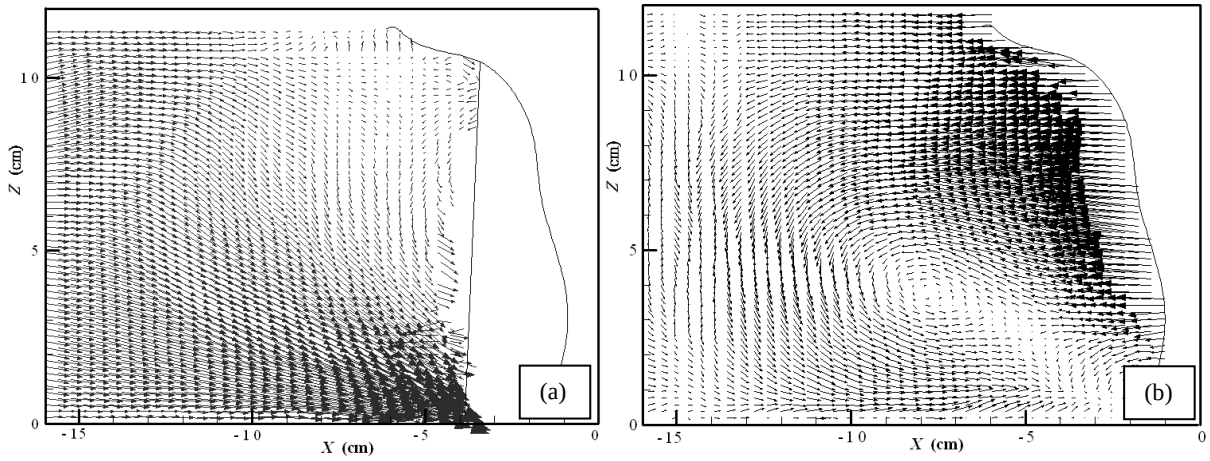

Figure 9. Velocity vector field of vertical PIV at: (a) Y = 0 cm; (b) Y = 6.5 cm.

Based on the observations from the vertical PIV velocity fields, it can be noted that where there is a recirculating cell, which is a section through the horizontal vortex tube, a mixing zone line can be expected upstream of the cell.

Theoretically, if there is a rotating cell downstream of the mixing line, there might be another rotating cell upstream of the mixing line rotating in the opposite direction.

3.3. Tangential Velocity Distribution in the Vortex Structure

Detailed velocity information was extracted from time averaged PIV velocity fields. Figure 10 shows the tangential velocity distribution (averaged over all radial directions) of the asymmetric air-core vortex at an elevation of 0.5 h compared to the models of Rankine (1858), Odgard (1986) and Mih (1990). In addition, the tangential velocity distribution of the vortex at four cardinal positions (0° ± 10°, 90° ± 10°, 180° ± 10°, and 270° ± 10°) at Z = 0.5h is plotted in Figure 10. The average tangential velocity profiles are similar in shape over the flow depth (0.25h and 0.75h not shown) with a higher peak velocity at 0.5h. The tangential profiles from the experimental data in Figure 10 are closest in shape to the Rankine Model but with a lower peak and difference in the logarithmically decreasing free vortex region outside the forced vortex core. This confirms the experimental results of Sun & Liu (2015) who observed the maximum tangential velocity of the air-core vortex at an elevation of Z = 0.58h.

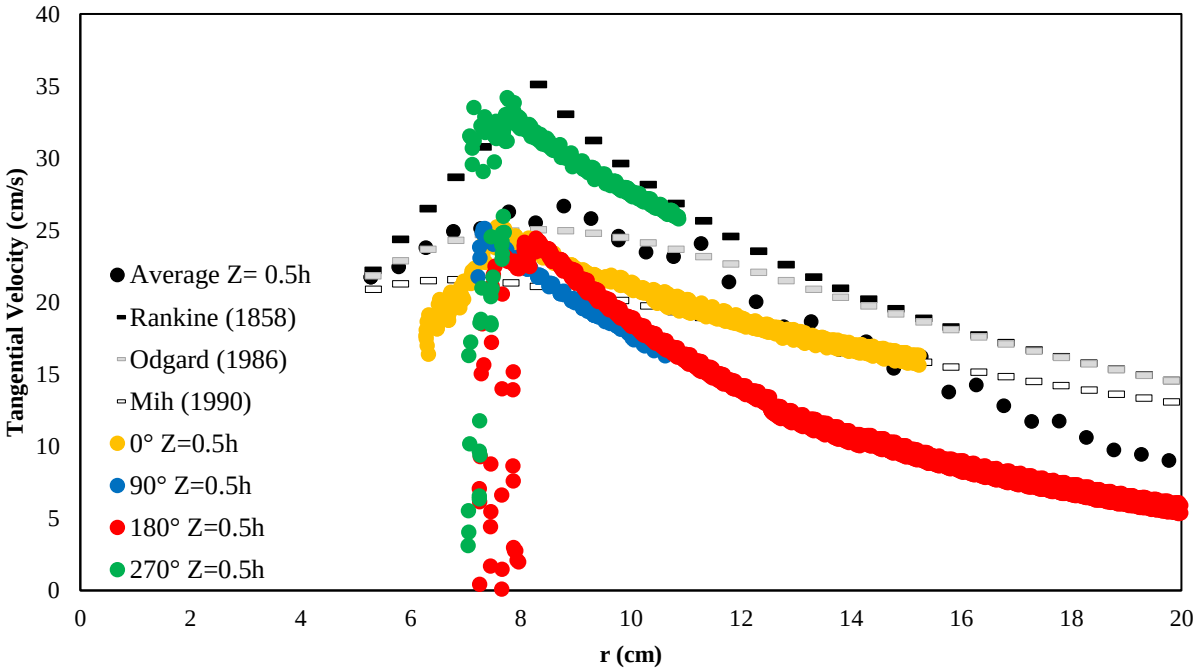

Figure 10. Tangential velocity distribution versus the radial direction.

The asymmetry of the vortex in the approach flow seen qualitatively in the flow visualizations is confirmed in the plots of the tangential velocity distributions determined at the four different radial positions (0°, 90°, 180° and 270°). The location of the peak tangential velocity is defined as the border of forced and free vortex zones. Its radial location is relatively constant at r = 8 cm and of similar magnitude (24 cm/s) except at 270° where it is higher (34 cm/s) due to the alignment of the tangential vortex and approach flow velocities. The rate of decrease in the magnitude of the tangential velocity is smaller downstream of the vortex than upstream of the vortex. This is due to the effect of the mixing zone upstream of the vortex and the region of alignment of the approach flow and tangential velocity leading up to the position downstream of the vortex.

4. Conclusion

The flow structure of a strong stable air-core vortex in an approach flow was studied using PIV and flow visualization techniques in both horizontal cross-sections and vertical sections. The interaction of the approach flow and the air-core vortex results in an asymmetrical vortex structure characterized by a mixing zone upstream of the vortex where the flows in opposing directions meet (approach flow velocity and tangential velocity of the vortex). This results in a

horizontal vortex forming along the diagonal line of the mixing zone at half depth, starting from the flume wall and joining the air-core vortex at its upstream edge. A rotating cell (-Y direction), a section of the horizontal curved vortex tube, was observed in the two vertical fields of view. This rotating cell splits the approach flow into two streams, one sweeping below with a higher velocity and the other flowing above at a lower velocity. The cross-sectional velocity data allowed for observation of the variation in the tangential velocity profiles, which confirms the asymmetry of the air-core vortex in an approach flow.

5. Acknowledgments

This work was conducted in collaboration with Professor Chang Lin, NCHU, Taiwan. We thank Prof. Lin who provided the test rig for the experiments. We would also like to show our gratitude to Mr. Ming-Han Kuo and Mr. Ming-Jer Kao who greatly assisted in this research.

6. References

Anwar, H.O., Weller, J.A., and Amphlett, M.B. (1978). "Similarity of free-vortex at horizontal intake." *Journal of Hydraulic Research*, 16(2), 95-105.

Burgers, J.M. (1948). "A mathematical model illustrating the theory of turbulence." *Advances in Applied Mechanics*. 1, 171–199.

Denny, D. F. (1956). "An experimental study of air-entraining vortices in pump sumps." *Proceedings of the Institution of Mechanical Engineers*, London, England, 170(1), 106-125.

Gulliver, J.S., and Rindels, A.J. (1987). "Weak vortices at vertical intakes." *Journal of Hydraulic Engineering*, ASCE 113(9), 1101–1116.

Hecker, G.E. (1987). Fundamentals of vortex intake flow. Conclusions. In: Knauss, J, editor. Swirling flow problems at intakes. IAHR hydraulic structures design manual. Rotterdam: Balkema, [chapters 2 and 8].

Hite, J.E., and Mih, W.C. (1994). "Velocity of air-core vortices at hydraulic intakes." *Journal of Hydraulic Engineering*, ASCE, 120(3), 284-297.

Jain, A.K., Rangaraju, K.G., and Garde, R.J. (1978). "Vortex formation at vertical pipe intakes." *Journal of the Hydraulics Division*. ASCE, 104(10), 1429–1448.

Li, H., Chen, H., Zheng, M.A., and Zhou, Y. (2008). "Experimental and numerical investigation of free surface vortex." *Journal of Hydrodynamics*. 20(4), 485-491.

Mih, W.C. (1990). "Analysis of fine particle concentrations in a combined vortex." Journal of Hydraulic Research, 28(3), 392-396.

Möller, G., Detert, M., and Boes R.M. (2015). "Vortex-induced air entrainment rates at intakes." *Journal of Hydraulic Engineering*, ASCE, 141(11), 04015026.

Mulligan, S., Casserly, J., and Sherlock, R. (2016). "Effects of Geometry on Strong Free-Surface Vortices in Subcritical Approach Flows." *Journal of Hydraulic Engineering*, ASCE, 142(11), 04016051.

Naderi, V., Farsadizadeh, D., Hosseinzadeh-Dalir, A., and Arvanaghi, H. (2013). "Experimental study of bell-mouth intakes on discharge coefficient." Journal of Civil Engineering *and Urbanism*, 3(6), 368-371.

Naderi, V., Farsadizadeh, D., Hosseinzadeh-Dalir, A., and Arvanaghi, H. (2014). "Effect of using vertical plates on vertical intake on discharge coefficient." *Arabian Journal for Science and Engineering*. 39(12), 8627-8633.

Odgaard, A.J. (1986). "Free-surface air core vortex". *Journal of Hydraulic Engineering*. ASCE, 112(7), 610-620.

Okamura, T., Kamemoto, K., and Matsui, J. (2007). "CFD prediction and model experiment on suction vortices in pump sump." *Proceedings of 9th Asian International Conference on Fluid Machinery*, October, Jeju, South Korea, AICFM9-053.

Rajendran, V.P. and Patel, V.C. (2000). "Measurement of vortices in model pump-intake bay by PIV." *Journal of Hydraulic Engineering*, ASCE, 126(5), 322–334.

Rankine, W.J.M. (1858). *A Manual of Applied Mechanics*, Charles Griffin, London.

Sarkardeh, H., Zarrati, A.R., and Roshan, R. (2010). "Effect of intake head wall and trash rack on vortices." *Journal of Hydraulic Research*, 48(1), 108-112.

Shemshi, R., and Kabiri-Samani, A. (2017) “Swirling flow at vertical shaft spillways with circular piano-key inlets.” *Journal of Hydraulic Research*, 55(2), 248-258.

Suerich-Gulick, F., Gaskin, S.J., Villeneuve, M., and Parkinson, E. (2014). “Free surface intake vortices: theoretical model and measurements.” *Journal of Hydraulic Research*, 52(4), 502-512.

Wang, Y.K., Jiang, C.B., and Liang, D.F. (2011). “Comparison between empirical formulae of intake vortices.” *Journal of Hydraulic Research*, 49(1), 113–116.